

# Homography-Based Visual Servoing of Wheeled Mobile Robots<sup>\*</sup>

<sup>1</sup>Y. Fang, <sup>1</sup>D. M. Dawson, <sup>2</sup>W. E. Dixon, and <sup>3</sup>M. S. de Queiroz

<sup>1</sup>Department of Electrical and Computer Engineering, Clemson University, Clemson, SC 29634-0915

<sup>2</sup>Eng. Science and Tech. Div. - Robotics, Oak Ridge National Laboratory, P.O. Box 2008, Oak Ridge, TN 37831-6305

<sup>3</sup>Department of Mechanical Engineering, Louisiana State University, Baton Rouge, LA 70803-6413

“The submitted manuscript has been authored by a contractor of the U.S. Government under contract DE-AC05-00OR22725. Accordingly, the U.S. Government retains a nonexclusive, royalty-free license to publish or reproduce the published form of this contribution, or allow others to do so, for U.S. Government purposes.”

To appear at the IEEE Conference on Decision and Control, Dec. 10-13, 2002, Las Vegas, Nevada

Keywords: Visual Servoing, Homography, Wheeled Mobile Robots, and  
Nonlinear Lyapunov-Based Control

E-mail: dixonwe@ornl.gov, Telephone: (865)574-9025

---

<sup>\*</sup> This research was supported in part by the Eugene P. Wigner Fellowship Program of the Oak Ridge National Laboratory (ORNL), managed by UT-Battelle, LLC, for the U.S. Department of Energy (DOE) under contract DE-AC05-00OR22725 and in part by the U.S. DOE Environmental Management Sciences Program (EMSP) projects ID No. 82794 and ID No. 82797 at ORNL, by ONR Project No. N00014-00-F-0485 at ORNL, and by U.S. NSF Grants DMI-9457967, DMI-9813213, EPS-9630167, ONR Grant N00014-99-1-0589, a DOC Grant, and an ARO Automotive Center Grant.

# Homography-Based Visual Servoing of Wheeled Mobile Robots\*

Y. Fang<sup>†</sup>, D. M. Dawson<sup>†</sup>, W. E. Dixon<sup>‡</sup>, and M. S. de Queiroz<sup>§</sup>

<sup>†</sup>Department of Electrical & Computer Engineering, Clemson University, Clemson, SC 29634-0915

<sup>‡</sup>Eng. Science and Tech. Div. - Robotics, Oak Ridge Nat. Lab., P.O. Box 2008, Oak Ridge, TN 37831-6305

<sup>§</sup>Department of Mechanical Engineering, Louisiana State University, Baton Rouge, LA 70803-6413

E-mail: yfang, ddawson@ces.clemson.edu; dixonwe@ornl.gov; dequeiroz@me.lsu.edu

## Abstract

By comparing the features of an object from a desired image to features of the object in the current image, geometric relationships are exploited to enable a Euclidean reconstruction from a homography matrix that relates the image-space feedback to the position/orientation of the wheeled mobile robot (WMR) in a local coordinate system. The information obtained from the homography is used to develop a kinematic controller that yields asymptotic regulation of the position/orientation of a WMR system that is modeled as an underactuated “kinematic wheel” subject to nonholonomic constraints. The control design is facilitated by performing the stability analysis in terms of the unmeasurable camera/WMR Euclidean position. In contrast to many of the previous homography-based visual servo controllers, the kinematic control law does not depend on the numerical estimation of depth measurements. The control design is based on the nonlinear model of the vision system and the mobile robot system and is analyzed through a Lyapunov-based stability analysis.

## 1 Introduction

Typically, wheeled mobile robots (WMRs) operate in environments that are either partially or completely unknown. Often the environment is changing with time in an unknown manner; hence, an intelligent sensor that can enable the robot to navigate in these environments is well motivated. Given this motivation, researchers initially targeted the use of sonar as an intelligent sensor. Based on the fact that sonar has very low-bandwidth capabilities, is subject to noise due to wave scattering, can be detected by external agents, and so on, researchers investigated the use of laser-based sensing. Although laser sensors have a much higher bandwidth, they are still subject to noise and are externally detectable. Moreover, lasers have a limited field-of-view, unless complexity such as rotating mirrors are incorporated in the sensor design. Given the

shortcomings of laser and sonar-based navigation, researchers investigated the use of camera-based systems (vision sensors). Vision sensors can have a wide field-of-view, can have millisecond sampling rates, and can be easily used for trajectory planning, and so on. However, some disadvantages of vision-based sensing include lack of depth information, image occlusion, low-resolution and the requirement for extensive data interpretation (image recognition). Given the advantages and disadvantages of the various sensors, some initial work targeted the use of a fusion of various sensors to build a map of the environment for WMR navigation (see [13, 15, 24, 25, 27] and the references within).

Based on the success of image extraction/interpretation technology and advances in control theory, more recent research has focused on the sole use of the vision system for navigating a WMR (although research related to laser and multi-sensor fusion is still a very active area of research). For example, using consecutive image frames and an object database, the authors of [14] recently proposed a WMR tracking controller based on monocular visual feedback. To achieve the result in [14], Kim et al. linearized the system equations using a Taylor series approximation, and then applied Extended Kalman Filtering (EKF) techniques. Also using EKF techniques on the linearized kinematic model, the authors of [7] used feedback from a monocular omnidirectional camera system (similar to [1]) to enable wall following, follow-the-leader, and position regulation tasks. In [12], Hager et al. used a monocular vision system mounted on a pan-tilt-unit to generate image-Jacobian and geometry-based controllers by using different snapshots of the target and an epipolar constraint. As stated in [2], a drawback of the method developed in [12] is that the system equations became numerically ill-conditioned for large pan angles. Given this shortcoming, Burschka and Hager [2] used a spherical image projection of a monocular vision system to overcome the limitations of [12]. Specifically, teaching and replay phases were used to facilitate the estimation of the unknown object height parameter in the image-Jacobian by solving a least-squares problem. In [23], Song and Huang, use spatiotemporal apparent velocities obtained from an optical flow of successive images of an object to estimate the depth and time-to-contact to develop a monocular vision “guide robot”. A similar optical flow technique was also developed in [16]. In [9], Dixon et al. used feedback from an uncalibrated, fixed (ceiling-mounted) camera to develop an adaptive tracking controller for a WMR that compensated for the parametric uncertainty in the camera and the WMR dynamics. In [26], Wang et al. exploited a rigid body

---

\*This research was supported in part by the Eugene P. Wigner Fellowship Program of the Oak Ridge National Laboratory (ORNL), managed by UT-Battelle, LLC, for the U.S. Department of Energy (DOE) under contract DE-AC05-00OR22725 and in part by the U.S. DOE Environmental Management Sciences Program (EMSP) projects ID No. 82794 and ID No. 82797 at ORNL, by ONR Project No. N00014-00-F-0485 at ORNL, and by U.S. NSF Grant DMI-9457967, ONR Grant N00014-99-1-0589, a DOC Grant, and an ARO Automotive Center Grant.

transformation to develop a visual servoing WMR tracking controller (the regulation problem was not solved due to restrictions on the reference trajectory) that adapted for the constant, unknown height of an object moving in a plane. In [29] and [17], visual servo controllers were recently developed for systems with similar underactuated kinematics as WMRs. Specifically, Mahony and Hamel [17] developed a semi-global asymptotic visual servoing result for unmanned aerial vehicles that tracked parallel co-planar linear visual features while Zhang and Ostrowski [29] used a vision system to navigate a blimp.

Recently, a monocular 2.5 Dimensional (2.5D) visual servo control methodology was developed in a series of papers by Malis and Chaumette (e.g., [3, 4, 19, 20]). Specifically, 2.5D visual servo exploits a combination of reconstructed 3D task-space information and 2D image-space information in the control design. The 3D information is reconstructed by decoupling the interaction between translation and rotation components of a Euclidean homography. As stated in [20], some of the advantages of this methodology include: (i) an accurate 3D model of the environment (or target image) is not required, (ii) the image is guaranteed to remain in the camera field-of-view, (iii) local minima can be avoided, and (iv) singularities only exist in the image-Jacobian in degenerate cases. Based on the observation that interaction between the translation and rotation of images can result in slower transient performance due to inefficient camera motions, Deguchi proposed two algorithms in [8] for a robot manipulator application that decouple the rotation and translation components using a homography and an epipolar condition. More recently, Corke and Hutchinson [6] also developed a method for decoupling the rotation and translation components from the remaining degrees of freedom using a new hybrid image-based visual servoing scheme. Unfortunately, the results given in [3, 4, 6, 8, 18, 19, 20] assume that a constant estimate of the depth information can be utilized in lieu of the exact value (e.g., in [20], an off-line learning stage is required to estimate the distance of the desired camera position to the reference plane for a robot manipulator application). Motivated by the desire to compensate for the aforementioned depth information, [5] developed an adaptive kinematic controller for a robot manipulator application to ensure uniformly ultimately bounded (UUB) set-point regulation of the image point errors while compensating for the unknown depth information, provided conditions on the translational velocity and the bounds on uncertain depth parameters are satisfied.

In this paper, asymptotic regulation of the position/orientation of a WMR is achieved by exploiting a homography-based visual servo control strategy inspired by the work given in [3, 4, 19, 20]. By comparing the features of an object in the desired image to features of the object in the current image (obtained from an onboard camera), geometric relationships are exploited to enable a Euclidean reconstruction from a Euclidean homography that relates the image-space feedback to the position/orientation of the camera/WMR in a local coordinate system. By decomposing the homography into separate translation and rotation components, measurable signals for the camera/WMR orientation and the scaled Euclidean position are obtained. The control objective for regulating the position/orientation of the WMR is naturally defined in terms of the Euclidean space, however, the Euclidean position error is unmeasurable. That is, the

Euclidean reconstruction is scaled by an unknown distance from the camera/WMR to the target, and while the scaled position is measurable through the homography, the unscaled position error is unmeasurable. To overcome this obstacle, a unique strategy is employed in which the kinematic control design is based on measurable 2D image-space information and reconstructed 3D information. The control design is facilitated by performing the stability analysis in terms of the unmeasurable camera/WMR Euclidean position. In contrast to many of the previous homography-based visual servo controllers, the kinematic control law developed in this paper does not depend on the calculation of the depth measurements. In contrast to visual servo methods that linearize the system equations to facilitate EKF methods, the Lyapunov-based control design in this paper is based on the full nonlinear model of the vision system and the mobile robot system.

## 2 Problem Formulation

The objective of this paper is to regulate the position/orientation of a WMR relative to a fixed target observed in the image-space. As illustrated in Figure 1, the origin of the orthogonal coordinate system  $\mathcal{F}$  attached to the camera is coincident with the center of mass of the WMR. As also illustrated in Figure 1, the XY-axis of  $\mathcal{F}$  defines the WMR plane of motion where the X-axis of  $\mathcal{F}$  is aligned with the front of the WMR, and the Y-axis is parallel to the wheel axis. The Z-axis of  $\mathcal{F}$  is perpendicular to the WMR plane of motion. The linear velocity of the WMR along the X-axis is denoted by  $v_c(t)$ , and the angular velocity  $\omega_c(t)$  is about the Z-axis. In addition to  $\mathcal{F}$ , another fixed orthogonal coordinate system, denoted by  $\mathcal{F}^*$ , is defined to represent the desired fixed position and orientation of the camera relative to a target. Hence, the goal is to develop a controller that will regulate the position and orientation of  $\mathcal{F}$  to  $\mathcal{F}^*$ .

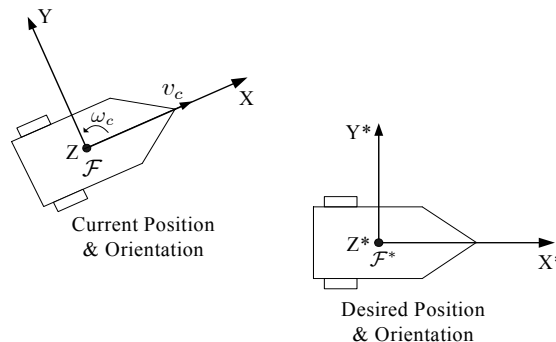


Figure 1: Mobile robot coordinate systems

### 2.1 Camera Model

In this paper, we assume that target can be distinguished by three points  $O_i$ ,  $i = 1, 2, 3$  that compose a plane, denoted by  $\pi$ . The Euclidean position of point  $O_i$  expressed in the coordinate frames  $\mathcal{F}$  and  $\mathcal{F}^*$  is denoted by  $\bar{m}_i(t), \bar{m}_i^* \in \mathbb{R}^3$ ,

respectively, and is defined as follows (see Figure 2)

$$\bar{m}_i(t) \triangleq [x_i(t) \ y_i(t) \ z_i(t)]^T \text{ and } \bar{m}_i^* \triangleq [x_i^* \ y_i^* \ z_i^*]^T. \quad (1)$$

Since the 3D Euclidean position of the points  $O_i$  are ob-

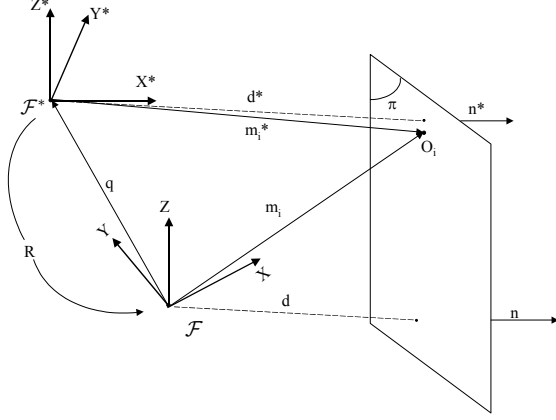


Figure 2: Geometric relationship of the mobile robot system

served from the 2D image-space of the camera, we define normalized position vectors  $m_i(t) \triangleq [1 \ m_{iy}(t) \ m_{iz}(t)]^T$ ,  $m_i^* \triangleq [1 \ m_{iy}^* \ m_{iz}^*]^T \in \mathbb{R}^3$  as follows

$$m_i(t) \triangleq \frac{\bar{m}_i(t)}{x_i(t)} = \begin{bmatrix} 1 & \frac{y_i(t)}{x_i(t)} & \frac{z_i(t)}{x_i(t)} \end{bmatrix}^T \quad (2)$$

$$m_i^* \triangleq \frac{\bar{m}_i^*}{x_i^*} = \begin{bmatrix} 1 & \frac{y_i^*}{x_i^*} & \frac{z_i^*}{x_i^*} \end{bmatrix}^T$$

where the standard assumption is made that  $x_i(t)$  and  $x_i^*$  are positive [20] (i.e., the target is always in front of the camera). In addition to the normalized Euclidean position, each of the points have an image-space representation, denoted by  $p_i(t), p_i^* \in \mathbb{R}^3$ , given by

$$p_i(t) \triangleq [1 \ u_i(t) \ v_i(t)]^T \quad p_i^* \triangleq [1 \ u_i^* \ v_i^*]^T. \quad (3)$$

The image-space coordinates given in (3) are related to the normalized coordinates given in (2) by the following invertible transformation

$$m_i = A^{-1}p_i \quad m_i^* = A^{-1}p_i^* \quad (4)$$

where  $A \in \mathbb{R}^{3 \times 3}$  denotes a constant, invertible matrix function of the intrinsic camera calibration parameters [20]. Since the camera is assumed to be calibrated (i.e., the matrix  $A$  is assumed to be known),  $m_i(t)$  and  $m_i^*$  can be calculated using (4) from the known camera pixel-space vectors  $p_i(t)$  and  $p_i^*$ .

The main idea behind the current visual servoing strategy is to extract 2D information from the environment using the camera image, and then estimate 3D information through a Euclidean reconstruction. The Euclidean reconstruction is performed by exploiting the geometry between the features of the target (image points) in the camera's current image to the desired image. Based on the geometric relationships, a homography matrix can then be calculated to relate the projected 3D position to the image-space position of the target [11, 20, 28].

For example, the geometric relationships between  $\mathcal{F}$  and  $\mathcal{F}^*$  can be determined from Figure 2 where  $\theta(t) \in \mathbb{R}$  is the angle between the axes  $X^*$  and  $X$ , the unit vectors  $n(t), n^* \in \mathbb{R}^3$  are normal to the plane  $\pi$  expressed in  $\mathcal{F}$  and  $\mathcal{F}^*$ , respectively, and  $d(t), d^* \in \mathbb{R}$  are the unknown, positive distances from the origin of  $\mathcal{F}$  and  $\mathcal{F}^*$  to the plane  $\pi$  along  $n$  and  $n^*$ , respectively. Based on Figure 2, the following relationship can be determined

$$\bar{m}_i = R\bar{m}_i^* + q \quad (5)$$

where  $R(t) \in SO(3)$  is the rotation matrix from  $\mathcal{F}^*$  to  $\mathcal{F}$  given by

$$R = \begin{bmatrix} \cos \theta & \sin \theta & 0 \\ -\sin \theta & \cos \theta & 0 \\ 0 & 0 & 1 \end{bmatrix} \quad (6)$$

and  $q(t) \in \mathbb{R}^3$  is the translation vector from  $\mathcal{F}$  to  $\mathcal{F}^*$  given by

$$q(t) = [q_x(t) \ q_y(t) \ 0]^T. \quad (7)$$

Since  $d^*$  is the projection of  $\bar{m}_i^*$  along  $n^*$ , the following relationship can be determined

$$d^* = (n^*)^T \bar{m}_i^*. \quad (8)$$

Using (8), the expression given in (5) can be rewritten as

$$\bar{m}_i = H\bar{m}_i^* \quad (9)$$

where the Euclidean homography  $H(t) \in \mathbb{R}^{3 \times 3}$  is defined as follows

$$H \triangleq R + \frac{q}{d^*} (n^*)^T. \quad (10)$$

By using (6), (7), and (10), the Euclidean homography can be rewritten as follows

$$H = [H_{jk}] = \begin{bmatrix} \cos \theta + \frac{q_x n_x^*}{d^*} & \sin \theta + \frac{q_x n_y^*}{d^*} & \frac{q_x n_z^*}{d^*} \\ -\sin \theta + \frac{q_y n_x^*}{d^*} & \cos \theta + \frac{q_y n_y^*}{d^*} & \frac{q_y n_z^*}{d^*} \\ 0 & 0 & 1 \end{bmatrix} \quad (11)$$

where  $n^* = [n_x^* \ n_y^* \ n_z^*]^T$ . Upon examination of the terms in (11), it is clear that  $H(t)$  contains signals that are not directly obtained from the vision system (e.g.,  $\theta(t)$ ,  $q(t)$ , and  $d^*$  are not directly available from the camera image). However, the six unknown elements of  $H_{jk}(t) \forall j = 1, 2, k = 1, 2, 3$  can be determined indirectly from the image coordinates by solving a set of linear equations. Specifically, by using the definition given in (2), the expression given in (9) can be rewritten as follows

$$m_i = \begin{pmatrix} x_i^* \\ x_i \end{pmatrix} H m_i^*. \quad (12)$$

By expanding (12), the following expressions can be obtained

$$1 = \begin{pmatrix} x_i^* \\ x_i \end{pmatrix} (H_{11} + H_{12}m_{iy}^* + H_{13}m_{iz}^*) \quad (13)$$

$$m_{iy} = \begin{pmatrix} x_i^* \\ x_i \end{pmatrix} (H_{21} + H_{22}m_{iy}^* + H_{23}m_{iz}^*) \quad (14)$$

$$m_{iz} = \begin{pmatrix} x_i^* \\ x_i \end{pmatrix} m_{iz}^*. \quad (15)$$

After eliminating (15), the following two expressions can be obtained

$$1 = \frac{m_{iz}}{m_{iz}^*} (H_{11} + H_{12}m_{iy}^* + H_{13}m_{iz}^*) \quad (16)$$

$$m_{iy} = \frac{m_{iz}}{m_{iz}^*} (H_{21} + H_{22}m_{iy}^* + H_{23}m_{iz}^*). \quad (17)$$

Given that (16) and (17) will be generated for each of the three image points, a total of six equations will result. Given the six equations, the six unknown elements of  $H_{jk}(t) \forall j = 1, 2, k = 1, 2, 3$  can be determined. Based on the fact that the elements of the homography matrix can be determined, various techniques can now be applied [11, 28] to decompose  $H(t)$  in terms  $R(t)$ ,  $\frac{q(t)}{d^*}$ , and  $n^*$  in (10); hence,  $\theta(t)$ ,  $n^*$ ,  $R(t)$ , and  $\frac{q(t)}{d^*}$  can be calculated and used in the subsequent control development. Note that while the ratio  $\frac{q(t)}{d^*}$  can be calculated, the individual signals  $q(t)$  and  $d^*$  are unmeasurable.

**Remark 1** *As stated previously, the homography-based visual servo control development exploits geometric relationships obtained from a desired image and the current image. Based on the fact that two images are used in the development, some heuristic parallels can be drawn between stereo-based vision problems and the homography-based problem. For example, the desired image obtained for the homography-based visual servo control problem can be thought of as being obtained from a constant, fixed (virtual) camera and the current image is obtained from the physical camera attached to the WMR. By using the virtual and physical camera images, a triangulation between the cameras and the object can be formulated as in Figure 2 to develop the Euclidean reconstruction. This approach seems similar to a stereo-vision approach; however, stereo-vision approaches require two physical cameras that have a known translation/rotation between the cameras.*

## 2.2 Control Objective

The goal of ensuring that  $\mathcal{F}$  coincides with  $\mathcal{F}^*$  is naturally defined in terms of the Euclidean position/orientation of the WMR. Specifically, the translation error between  $\mathcal{F}$  and  $\mathcal{F}^*$ , denoted by  $e_t(t) \in \mathbb{R}^2$ , can be written for any of the image points  $O_i$ ,  $i = 1, 2, 3$  as follows

$$e_t \triangleq \begin{bmatrix} e_{tx} \\ e_{ty} \end{bmatrix} = \begin{bmatrix} q_x \\ q_y \end{bmatrix} = \begin{bmatrix} x_i \\ y_i \end{bmatrix} - \begin{bmatrix} \cos \theta & \sin \theta \\ -\sin \theta & \cos \theta \end{bmatrix} \begin{bmatrix} x_i^* \\ y_i^* \end{bmatrix} \quad (18)$$

where (5), (6), and (7) have been utilized. The orientation error between  $\mathcal{F}$  and  $\mathcal{F}^*$ , denoted by  $e_o(t) \in \mathbb{R}$ , can be written as follows

$$e_o(t) \triangleq \theta(t) \quad (19)$$

where  $\theta$  was defined in (6). Based on the definitions of (18) and (19), the control objective can be stated as ensuring that  $e_t(t)$  and  $e_o(t)$  are regulated to zero.

## 3 Control Development

### 3.1 Open-Loop Error System

To develop the kinematic controller, we first examine the open-loop error system for the error signals  $e_t(t)$  and  $e_o(t)$ . To this end, we take the time derivative of (18) and (19) as follows

$$\begin{bmatrix} \dot{e}_{tx} \\ \dot{e}_{ty} \end{bmatrix} = \begin{bmatrix} \dot{x}_i \\ \dot{y}_i \end{bmatrix} - \begin{bmatrix} -\sin \theta & \cos \theta \\ -\cos \theta & -\sin \theta \end{bmatrix} \begin{bmatrix} x_i^* \\ y_i^* \end{bmatrix} \dot{\theta} \quad (20)$$

$$\dot{e}_o = \dot{\theta}.$$

As stated in [8, 20], the time derivative of the Euclidean position given in (1) can be determined as follows

$$\dot{\bar{m}}_i = -v - \omega \times \bar{m}_i, \quad (21)$$

where  $v(t), \omega(t) \in \mathbb{R}$  denote the linear and angular velocity of the WMR expressed in  $\mathcal{F}$  as

$$v(t) \triangleq \begin{bmatrix} v_c(t) & 0 & 0 \end{bmatrix}^T \quad (22)$$

$$\omega(t) \triangleq \begin{bmatrix} 0 & 0 & \omega_c(t) \end{bmatrix}^T = \begin{bmatrix} 0 & 0 & \dot{\theta}(t) \end{bmatrix}^T,$$

respectively. From the expression given in (1) and (21), the Euclidean WMR velocity can be written in terms of the linear and angular velocity as follows

$$\begin{aligned} \dot{x}_i &= -v_c + y_i \omega_c \\ \dot{y}_i &= -x_i \omega_c. \end{aligned} \quad (23)$$

After substituting (23) and (22) into (20), the following open-loop error system for  $e_t(t)$  and  $e_o(t)$  can be determined

$$\begin{aligned} \dot{e}_{tx} &= -v_c + \omega_c e_{ty} \\ \dot{e}_{ty} &= -\omega_c e_{tx} \\ \dot{e}_o &= \omega_c \end{aligned} \quad (24)$$

where (18) was utilized.

### 3.2 Control Design

Based on the form of (24) and the subsequent stability analysis, the kinematic control inputs  $v_c(t)$  and  $\omega_c(t)$  can be designed in a similar manner as in [21] as follows

$$v_c = k_v \frac{e_{tx}}{x_i^*} \quad \text{and} \quad \omega_c = -k_{\omega 1} e_o + k_{\omega 2} \left( \frac{e_{ty}}{x_i^*} \right)^2 \sin(t) \quad (25)$$

where  $k_v, k_{\omega 1}, k_{\omega 2} \in \mathbb{R}$  denote positive, constant control gains. Although the control design given in (25) is well motivated by the subsequent stability analysis, it is important to note that the expressions for  $v_c(t)$  and  $\omega_c(t)$  given in (25) cannot be implemented due to the fact that  $e_t(t)$  and  $x_i^*$  are unmeasurable. We note that  $e_o(t)$  can be calculated from the decomposed homography matrix as follows

$$\cos \theta = \frac{1}{2} (\text{tr}(R) - 1). \quad (26)$$

Motivated by the desire to express the controller given in (25) in terms of measurable signals, we substitute (18) into (25) for the unmeasurable Euclidean position  $e_t(t)$  to obtain the following expression

$$\begin{aligned} v_c &= k_v \left( \frac{x_i}{x_i^*} - \cos \theta - m_{iy}^* \sin \theta \right) \\ \omega_c &= -k_{\omega 1} e_o + k_{\omega 2} \left( \frac{x_i}{x_i^*} m_{iy} + \sin \theta - m_{iy}^* \cos \theta \right)^2 \sin(t) \end{aligned} \quad (27)$$

where (2) was utilized. In Appendix A, we illustrate that the ratio  $\frac{x_i(t)}{x_i^*}$  can be written in the following form

$$\frac{x_i}{x_i^*} = \frac{(n^*)^T m_i^*}{(n^*)^T R^T m_i} \left[ 1 + (n^*)^T R^T \left( \frac{q}{d^*} \right) \right] \quad (28)$$

where, as stated previously,  $n^*$ ,  $R(t)$ , and  $\frac{q(t)}{d^*}$  can be calculated from the decomposed homography matrix. Hence, the expressions given in (27) and (28) represent a measurable form of the kinematic control  $v_c(t)$  and  $\omega_c(t)$ . By substituting the equivalent unmeasurable control expression given in (25) into (24), the following closed-loop error system is obtained

$$\begin{aligned}\dot{e}_{tx} &= -k_v \frac{e_{tx}}{x_i^*} + \omega_c e_{ty} \\ \dot{e}_{ty} &= -\omega_c e_{tx} \\ \dot{e}_o &= -k_{\omega 1} e_o + k_{\omega 2} \left( \frac{e_{ty}}{x_i^*} \right)^2 \sin(t).\end{aligned}\quad (29)$$

**Remark 2** *The above closed-loop system for  $e_o(t)$  represents a stable linear system subject to the disturbance  $k_{\omega 2} \left( \frac{e_{ty}(t)}{x_i^*} \right)^2 \sin(t)$ ; hence,  $e_o(t)$  is bounded provided the disturbance is bounded. Furthermore, if*

$$\lim_{t \rightarrow \infty} e_{ty}(t) = 0 \quad (30)$$

then it is clear that

$$\lim_{t \rightarrow \infty} e_o(t) = 0. \quad (31)$$

### 3.3 Stability Analysis

**Theorem 1** *The control law given in (27) and (28) ensures that the position and orientation of the WMR coordinate frame  $\mathcal{F}$  is regulated to the desired position/orientation described by  $\mathcal{F}^*$  in the sense that*

$$\lim_{t \rightarrow \infty} e_t(t), e_o(t) = 0. \quad (32)$$

**Proof.** To prove (32), we define a non-negative function  $V(t)$  as follows

$$V \triangleq \frac{1}{2} e_t^T e_t. \quad (33)$$

After taking the time derivative of (33) and then substituting the closed-loop error system given in (29) into the resulting expression, we obtain

$$\dot{V} = -\frac{k_v}{x_i^*} e_{tx}^2. \quad (34)$$

The expressions given in (33) and (34) can be used to prove that  $e_t(t) \in \mathcal{L}_\infty$  and that  $e_{tx}(t) \in \mathcal{L}_2$ . Based on the fact that  $e_t(t) \in \mathcal{L}_\infty$ , the arguments given in Remark 2 can be used to prove that  $e_o(t) \in \mathcal{L}_\infty$ . After utilizing (2), (18), (24), and (27), we can prove that  $x_i(t)$ ,  $y_i(t)$ ,  $m_{iy}(t)$ ,  $v_c(t)$ ,  $w_c(t)$ ,  $\dot{e}_t(t)$ , and  $\dot{e}_o(t) \in \mathcal{L}_\infty$ . Based on the fact that  $e_t(t)$ ,  $e_o(t)$ ,  $\dot{e}_t(t)$ , and  $\dot{e}_o(t) \in \mathcal{L}_\infty$  and that  $e_{tx}(t) \in \mathcal{L}_2$ , Barbalat's lemma [22] can be employed to prove that

$$\lim_{t \rightarrow \infty} e_{tx}(t) = 0. \quad (35)$$

From the closed-loop error system given in (29), (35) can be used to prove that

$$\lim_{t \rightarrow \infty} \dot{e}_{ty}(t) = 0. \quad (36)$$

After taking the time derivative of the product  $e_{tx}(t)e_{ty}(t)$  and substituting (29) into the resulting expression, we obtain

$$\frac{d}{dt} (e_{tx}e_{ty}) = e_{ty}^2 \omega_c + e_{tx} \left( \dot{e}_{ty} - k_v \frac{e_{ty}}{x_i^*} \right). \quad (37)$$

From (35) and the fact that the signal  $e_{ty}^2(t)\omega_c(t)$  is uniformly continuous,<sup>1</sup> we can invoke the Extended Barbalat's Lemma [10] to prove that

$$\lim_{t \rightarrow \infty} \frac{d}{dt} (e_{tx}(t)e_{ty}(t)) = 0 \quad (38)$$

and that

$$\lim_{t \rightarrow \infty} e_{ty}(t)\omega_c(t) = 0. \quad (39)$$

After taking the time derivative of the product  $e_{ty}(t)\omega_c(t)$ , and then utilizing (25) and (29), the following expression can be obtained

$$\begin{aligned}\frac{d}{dt} (e_{ty}\omega_c) &= k_{\omega 2} \frac{e_{ty}^3}{x_i^{*2}} \cos(t) \\ &+ \left[ \dot{e}_{ty} \left( \omega_c + 2k_{\omega 2} \frac{e_{ty}^2}{x_i^{*2}} \sin(t) \right) - k_{\omega 1} e_{ty}\omega_c \right].\end{aligned}\quad (40)$$

Based on (36) and (39), the bracketed term of (40) goes to zero as  $t \rightarrow \infty$ . Therefore, since the term  $\frac{e_{ty}^3(t)}{x_i^{*2}} \cos(t)$  is uniformly continuous (since  $e_t(t)$ ,  $\dot{e}_t(t) \in \mathcal{L}_\infty$ ), the Extended Barbalat's Lemma [10] can be invoked again to prove that

$$\lim_{t \rightarrow \infty} \frac{e_{ty}^3(t)}{x_i^{*2}} \cos(t) = 0, \quad (41)$$

which implies that

$$\lim_{t \rightarrow \infty} e_{ty}(t) = 0. \quad (42)$$

From (42) and the arguments given in Remark 2, we can now prove that

$$\lim_{t \rightarrow \infty} e_o(t) = 0 \quad \square. \quad (43)$$

## 4 Conclusion

In this paper, asymptotic regulation of the position/orientation of a WMR is achieved with a monocular vision system. By comparing the features of an object from an initial snapshot to features of the object in the current image, geometric relationships are exploited to determine a Euclidean homography that relates the image-space feedback to the actual Euclidean position/orientation of the camera (and hence the WMR) in a local coordinate system. By decomposing the homography into separate translation and rotation components, we were able to exploit reconstructed 3D task-space information to construct the kinematic controller. The control design is facilitated by performing the stability analysis in terms of the unmeasurable camera/WMR Euclidean position. Our future efforts will target the development of analytical methods that enable adaptive/robust techniques to be employed to compensate for the uncertainty associated with the camera calibration parameters. Future efforts will also target real-time experimental demonstration of the proposed controllers using a Cybermotion K2A mobile robot and a Dalsa CAD 6 camera capable of capturing 955 frames per second.

## References

- [1] S. Baker and S. Nayar, "A Theory of Catadioptric Image Formation," *Proc. of the ICCV*, pp. 35-42, Jan. 1998.

<sup>1</sup>Since  $e_t(t)$ ,  $\dot{e}_t(t)$ ,  $\dot{e}_o(t) \in \mathcal{L}_\infty$ , (25) can be used to prove that  $\dot{\omega}_c(t) \in \mathcal{L}_\infty$ , and hence,  $\omega_c(t)$  is uniformly continuous.

- [2] D. Burschka and G. Hager, "Vision-Based Control of Mobile Robots," *Proc. of the IEEE International Conference on Robotics and Automation*, pp. 1707-1713, 2001.
- [3] F. Chaumette and E. Malis, "2 1/2 D visual servoing: a possible solution to improve image-based and position-based visual servoings," *Proc. of the IEEE International Conference on Robotics and Automation*, pp. 630-635, 2000.
- [4] F. Chaumette, E. Malis, and S. Boudet, "2D 1/2 Visual Servoing With Respect to a Planar Object," *Proc. of the Workshop on New Trends in Image-Based Robot Servoing*, pp. 45-52, 1997.
- [5] F. Conticelli and B. Alotta, "Nonlinear Controllability and Stability Analysis of Adaptive Image-Based Systems," *IEEE Transactions on Robotics and Automation*, Vol. 17, No. 2, April 2001.
- [6] P. I. Corke and S. A. Hutchinson, "A New Hybrid Image-Based Visual Servo Control Scheme," *Proc. of the IEEE Conference on Decision and Control*, pp. 2521-2527, 2000.
- [7] A. K. Das, et al., "Real-Time Vision-Based Control of a Non-holonomic Mobile Robot," *Proc. of the IEEE International Conference on Robotics and Automation*, pp. 1714-1719, 2001.
- [8] K. Deguchi, "Optimal Motion Control for Image-Based Visual Servoing by Decoupling Translation and Rotation," *Proceedings of the Intl. Conf. on Intelligent Robots and Systems*, B.C. Canada, pp. 705-711, Oct. 1998.
- [9] W. E. Dixon, D. M. Dawson, E. Zergeroglu, and A. Behal, "Adaptive Tracking Control of a Wheeled Mobile Robot via an Uncalibrated Camera System," *Proc. of the IEEE American Control Conference*, Chicago, Illinois, June, 2000, pp. 1493-1497.
- [10] W. E. Dixon, D. M. Dawson, E. Zergeroglu and A. Behal, *Nonlinear Control of Wheeled Mobile Robots*, Springer-Verlag London Limited, 2001.
- [11] O. Faugeras and F. Lustman, "Motion and structure from motion in a piecewise planar environment," *International Journal of Pattern Recognition and Artificial Intelligence*, Vol. 2, No. 3, pp. 485-508, 1988.
- [12] G. D. Hagar, D. J. Kriegman, A. S. Georghiadis, and O. Ben-Shahar, "Toward Domain-Independent Navigation: Dynamic Vision and Control," *Proc. of the IEEE Conference on Decision and Control*, pp. 3257-3262, 1998.
- [13] M. Hebert, "3-D vision for outdoor navigation by an autonomous vehicle," *Proc. of the Image Understanding Workshop*, Cambridge, UK, 1998.
- [14] B. H. Kim, et al., "Localization of a Mobile Robot using Images of a Moving Target," *Proc. of the IEEE International Conference on Robotics and Automation*, pp. 253-258, 2001.
- [15] D. J. Kriegman, E. Triendl, and T. O. Binford, "Stereo Vision Navigation in Buildings for Mobile Robots," *IEEE Transactions on Robotics and Automation*, Vol. 5, No. 6, pp. 792-803, Dec. 1989.
- [16] Y. Ma, J. Kosecka, and S. Sastry, "Vision Guided Navigation for Nonholonomic Mobile Robot", *IEEE Trans. on robotics and Automation*, Vol. 15, No. 3, pp. 521-536, June 1999.
- [17] R. Mahony and T. Hamel, "Visual Servoing Using Linear Features for Under-actuated Rigid Body Dynamics," *Proc. of the IEEE/RJS International Conference on Intelligent Robots and Systems*, pp. 1153-1158, 2001.
- [18] E. Malis, "Contributions à la modélisation et à la commande en asservissement visuel," Ph.D. Dissertation, University of Rennes I, IRISA, France, Nov. 1998.
- [19] E. Malis and F. Chaumette, "2 1/2 D visual servoing with respect to unknown objects through a new estimation scheme of camera displacement," *International Journal of Computer Vision*, pp. 79-97, Vol. 37, No. 1, June 2000.
- [20] E. Malis, F. Chaumette, and S. Bodet, "2 1/2 D Visual Servoing," *IEEE Transactions on Robotics and Automation*, pp. 238-250, Vol. 15, No. 2, April 1999.
- [21] C. Samson, "Velocity and Torque Feedback Control of a Non-holonomic Cart," *Proc. International Workshop in Adaptive and Nonlinear Control: Issues in Robotics*, Grenoble, France, 1990.
- [22] J. J. Slotine and W. Li, *Applied Nonlinear Control*, Englewood Cliff, NJ: Prentice Hall, Inc., 1991.
- [23] K.-T. Song and J.-H. Huang, "Fast Optical Flow Estimation and Its Application to Real-time Obstacle Avoidance," *Proc. of the IEEE International Conference on Robotics and Automation*, pp. 2891-2896, 2001.
- [24] C. E. Thorpe, M. Hebert, T. Kanade, and S. Shafer, "Vision and Navigation for the Carnegie-Mellon Navlab," *IEEE Trans. Pattern Anal. Machine Intell.*, Vol. 10, No. 3, pp. 362-373, May 1988.
- [25] M. A. Turk, D. G. Morgenthaler, K. D. Gremban, and M. Marra, "VITS-A Vision System for Autonomous Land Vehicle Navigation," *IEEE Trans. Pattern Anal. Machine Intell.*, Vol. 10, No. 3, pp. 342-361, May 1988.
- [26] H. Y. Wang, S. Itani, T. Fukao, and N. Adachi, "Image-Based Visual Adaptive Tracking Control of Nonholonomic Mobile Robots", *Proc. of the IEEE/RJS International Conference on Intelligent Robots and Systems*, pp. 1-6, 2001.
- [27] A. M. Waxman, et al., "A Visual Navigation System for Autonomous Land Vehicles," *IEEE Journal of Robotics Automation*, Vol. RA-3, No. 2, pp. 124-141, 1987.
- [28] Z. Zhang and A. R. Hanson, "Scaled Euclidean 3D Reconstruction Based on Externally Uncalibrated Cameras," *IEEE Symp. on Computer Vision*, 1995.
- [29] H. Zhang and J. P. Ostrowski, "Visual Servoing with Dynamics: Control of an Unmanned Blimp," *Proc. of the IEEE International Conference on Robotics and Automation*, pp. 618-623, 1999.

## 5 Appendix A

By using the geometric relationships given in Figure 2, it is clear that  $d$  is the projection of  $\bar{m}_i(t)$  along  $n(t)$ , and hence, (2) can be used to show that

$$d = n^T \bar{m}_i = n^T m_i x_i. \quad (44)$$

Likewise, from (8), the following expression can be obtained

$$d^* = (n^*)^T m_i^* x_i^*. \quad (45)$$

After dividing (44) by (45) and then rearranging the resulting equation, the following expression can be obtained

$$\frac{x_i}{x_i^*} = \frac{(n^*)^T m_i^*}{n^T m_i} \left( \frac{d}{d^*} \right). \quad (46)$$

From the geometry given in Figure 2, it can also be determined that

$$d = d^* + n^T q. \quad (47)$$

After dividing (47) by  $d^*$ , the following expression can be obtained

$$\frac{d}{d^*} = 1 + n^T \frac{q}{d^*}. \quad (48)$$

Substituting (48) into (46) and then making use of the fact that  $n = Rn^*$  yields

$$\frac{x_i}{x_i^*} = \frac{(n^*)^T m_i^*}{(n^*)^T R^T m_i} \left[ 1 + (n^*)^T R^T \left( \frac{q}{d^*} \right) \right]. \quad (49)$$